Soft Matter

PAPER

Cite this: *Soft Matter*, 2017, **13**, 8492

Soft polyhedral particles based on cubic liquid crystalline emulsion droplets†

Haiqiao Wang,[ab] Per B. Zetterlund,[b] Cyrille Boyer,[b] Ben J. Boyd,[c] Stuart W. Prescott[a] and Patrick T. Spicer*[a]

Received 31st July 2017,
Accepted 25th October 2017

DOI: 10.1039/c7sm01521f

rsc.li/soft-matter-journal

Soft polyhedral particles based on variations of the cubic symmetry group are produced from a precursor emulsion by extracting solvent to grow facets on the droplets. The droplets transform into liquid crystals with solid-like rheology and controlled size and shape. Small-angle X-ray scattering confirms a bicontinuous cubic liquid crystalline phase forms from aqueous glycerol monoolein and is responsible for the particle faceting observed. Different polyhedra are produced by varying face growth rates through control of precursor droplet size, system temperature, and solubilization and adsorption of guest molecules. More exotic faceted shapes can be formed by the soft particles by applying asymmetric solvent removal gradients and by deforming the precursor droplets into, for example, ellipsoids before crystallization. The method is a powerful means to produce soft polyhedra, using continuous microfluidic or other approaches, or to act as templates for hard polyhedral particle synthesis.

1 Introduction

Controlled formation of complex particle shapes has emerged as a powerful motivation for research in development areas like acoustic metamaterials,[1] rheology control,[2] and drug delivery.[3–8] Just as biological cells vary widely in shape depending on function, synthetic particles can form a number of complex shapes *via* diverse methods.[9] Simple geometric shapes have been synthesized in a number of ways, but more complex shapes enable sophisticated hierarchical particle self-assembly. A crucial trait is particle faceting, as it tunes short-range interactions and directs dispersed particles to form preferred assemblies.[10,11] Simulations[10] can access any shape, as well as intermediates between shapes, but realisation of theoretical targets requires an experimental system as flexible as a simulation in its ability to produce and optimise complex particle shapes. For the ultimate flexibility, we need a system that can form many different shapes, retain different facet structures, and remain soft enough to allow more complex customisation than solids. An experimental toolkit of widely variable polyhedral particles is needed to achieve the ambitious vision set for faceted particle assemblies.[10,12–15]

Excellent methods exist to synthesize solid particles with pre-designed shapes[16,17] or buckled forms,[18] but faceted particles can require crystallization[13,19,20] or specific molecular synthetic methods.[21] Softer materials like viscoelastic hydrogels have rheology that allows creation of faceted particles *via* molding[22] and buckling[23] but lose their fluid character in the process. Interfacial tension normally limits liquid droplet shapes to spheres, but is offset by interfacial[24,25] or internal elasticity[26–28] to form stable non-spherical shapes. Droplet faceting requires elasticity combined with an underlying structural order, as when interfacial crystallization on droplets[29–31] produces faceted solid capsules. A new approach is the use of liquid crystalline droplets, as they uniquely combine fluid-like rheology, crystalline faceting, and production simplicity.

Certain lyotropic liquid crystalline phases behave as a solid with an elastic modulus, $G' \sim 10^5$ Pa[32] at stresses below their yield stress, while flowing like a viscous liquid above it.[32,33] Hexagonal and bicontinuous cubic phases form stable dispersed liquid crystalline nanoparticles, hexosomes and cubosomes, are useful as drug delivery vehicles[34–38] and form faceted shapes with length scales ~100 nm,[39–42] though control of particle shape in these systems is not currently possible. Recent studies of complex facet formation in single large hemispherical droplets of smectic,[43] nematic,[44] and cubic lyotropic liquid crystalline phases[45] suggest an elegant way to produce beautifully complex faceted particles.[46] What is needed is a way to more flexibly control the shape of such particles, in three dimensions, *via* a robust, scalable process.

We describe here the production of soft, faceted, three-dimensionally symmetric particles using carefully tuned fluid rheology and adsorption to control particle size and shape.

[a] *Complex Fluids Group, School of Chemical Engineering, UNSW Sydney, Australia. E-mail: p.spicer@unsw.edu.au*
[b] *Centre for Advanced Macromolecular Design, School of Chemical Engineering, UNSW Sydney, Australia*
[c] *Drug Delivery, Disposition and Dynamics and ARC Centre of Excellence in Convergent Bio-Nano Science and Technology, Monash Institute of Pharmaceutical Sciences, Monash University (Parkville Campus), 381 Royal Pde, Parkville, Victoria 3052, Australia*

† Electronic supplementary information (ESI) available. See DOI: 10.1039/c7sm01521f

The method is designed to enable continuous flow production of faceted particles in practical mixing systems, and is carried out using edible, safe materials and simple processes.

2 Experimental

Commercial grade monoolein, Dimodan MO90K, was obtained from DuPont Danisco (Botany, NSW, Australia). The phase behavior of this system matches that of pure monoolein, in agreement with our earlier work[40] and consistent with more detailed studies.[47] The additives 99% ethanol and Pluronic F-127 were purchased from Sigma Aldrich (Castle Hill, NSW, Australia). Microfibrillated cellulose, MFC, was purchased from Wong Coco (Jakarta, Indonesia). Carbopol 846 was obtained from Lubrizol (Silverwater, NSW, Australia). All chemicals were used without further purification. Ultra-pure water with a resistivity of 18.25 MΩ cm was obtained using a Sartorius Ultrapure water purifier.

Polyhedral particles were formed by combination of a precursor solution and a diluting solution, whose composition varies depending on the desired particle type. All precursor solutions contained 55 wt% monoolein, 25% ethanol, and 20% water, indicated by point A in Fig. 1. All experiments were conducted at 25 °C unless otherwise stated.

Initially, 0.02–0.2 mL of precursor was injected with a syringe into 3.5 mL of a diluting solution containing water, ethanol, and 0.1% w/w rheological modifier, MFC, that adds a yield stress to the fluid. A second yield stress fluid, aqueous Carbopol 846, was used as the continuous phase fluid when surface adsorption effects were needed. The ethanol concentration in the diluting solution was 25% v/v unless otherwise specified. Mixing the two solutions forms emulsion droplets that are then transformed into polyhedra by evaporation of ethanol from the suspension.

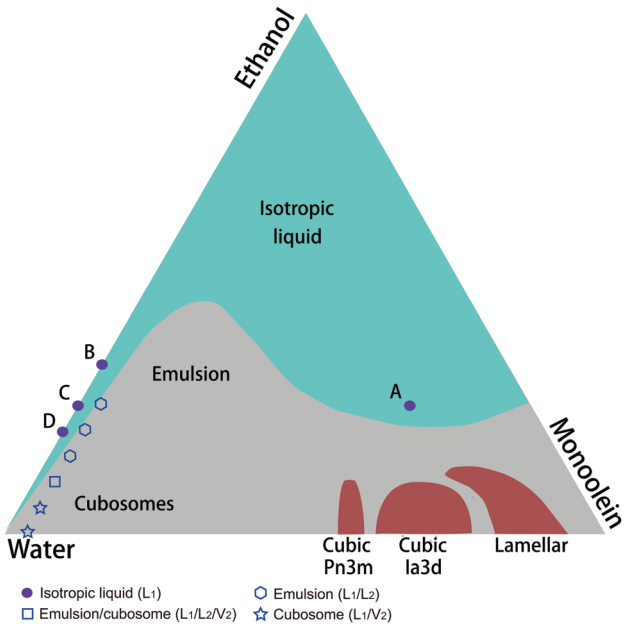

Fig. 1 Pseudo-ternary phase diagram for the monoolein–ethanol–water system[40] used here to make polyhedra. Closed symbols indicate the compositions of the precursor solution, A, and a diluting solution with 33%, B, 25%, C, or 20%, D, ethanol. Open symbols show specific bulk results for multiple-phase regions relevant to the formation of particles.

Some production of larger numbers of precursor droplets was performed using a simple millifluidic device made from coaxially aligned capillaries.[48,49] Precursor solution flows in the inner cylindrical capillary with an inner diameter of 100 μm. Diluting solution flows in the outer cylindrical capillary with an inner diameter of 1.6 mm. Both liquids are injected using syringe pumps (WPI, 947-371-1003) using flow rates of 0.5 μL min^{-1} and 1 mL min^{-1} for precursor and diluting solutions, respectively.

All particle formation experiments were carried out with samples in an open petri dish with a liquid height of 4 mm and a free surface area of 9.6 cm^2 to facilitate evaporation of ethanol and induce liquid crystal formation. The sample was held at constant T = 25 °C and relative humidity = 60% in a static environment during the transition process from droplets to particles. Adjusting the driving force of temperature or ethanol concentration, for example, can change the solvent evaporation rate, if desired. Measurements of mass loss with time were carried out using a Shimadzu TW423L balance in a controlled temperature and humidity environment. All time-dependent microscopic and SAXS measurements were performed by sampling from the petri dish containing the suspension. Once the desired shapes were formed, the suspending yield stress matrix was diluted for easy particle recovery.

Microscope observations were conducted on a Leica DM2500M optical microscope and all images were recorded using a Moticam 10 MP digital camera. Micrographs shown here portray shapes representative of dispersions of more than 100 particles in a sample. Synchrotron small-angle X-ray scattering, SAXS, was used to identify the liquid crystalline structures responsible for larger-scale symmetry and faceting of all particles produced here. Samples were sealed into flat quartz cells mounted vertically on a remotely operated X–Y–Z translation stage at the Australian Synchrotron SAXS/WAXS beamline[50] and exposed to an X-ray beam with a wavelength of 1.12 Å, energy 11 keV, with a sample-to-detector distance of 1034 mm. This setup provides a q range from $0.018 < q < 1.02$ $Å^{-1}$, where q is the magnitude of the scattering vector, defined as $q = 4\pi/\lambda \sin(\theta/2)$, λ is the radiation wavelength, and θ the scattering angle. Two-dimensional spatial-resolved SAXS patterns were collected using 100 μm steps on the translation stage, with 1 s acquisition at each position. A Pilatus 1 M detector with an active area of 169 × 179 mm^2 and a pixel size of 172 μm was used for acquisition. The two-dimensional SAXS patterns were then integrated into a one-dimensional scattering function $I(q)$ using ScatterBrain Analysis software.[51]

3 Results and discussion

The phase diagram in Fig. 1 maps the pseudo-ternary monoolein–ethanol–water system used here. A large single phase region of isotropic liquid, L_1, is mapped in Fig. 1 as a turquoise region, and is the basis for a precursor solution to form particles. The system contains three liquid crystalline phases,

in red regions, two of which are inverse bicontinuous cubic phases, V_2, and one lamellar phase, L_α.[40] Past work showed that nanoparticle cubosomes can be formed directly by homogeneous nucleation during dilution of the isotropic phase, L_1, into the water-rich region of the system,[40] marked "cubosomes" in Fig. 1. The process is simple, and avoids the need for high-energy dispersion of viscous bulk cubic phase, but produces a broad particle size distribution spanning nanometers to microns.

Here we altered the bottom-up process to pass through an emulsion intermediate to better control particle size and carefully study facet formation. Instead of diluting with water alone,[40] we diluted with a mixture of ethanol and water. The production of particles occurs in two stages: emulsion formation followed by evaporation of ethanol from the droplets to form liquid crystal particles. In the first stage, emulsion droplets of concentrated isotropic L_2 phase form in a continuous phase of dilute L_1 isotropic phase when the two precursor solutions are combined, in the area labeled "emulsion" in Fig. 1. The two-phase region is located on the dilution trajectory connecting the precursor composition marked A and one of three diluting solutions marked B, C, and D. Formation of polyhedral particles then requires moving from the two-phase emulsion to the two-phase cubic *Pn3m*-L_1 system by evaporative removal of ethanol. Phase equilibria require a change in the number of phases during such a transition, meaning the system passes through a three-phase intermediate state: the L_2-*Pn3m*-L_1 system.[46] Relative locations of these states are shown in the phase diagram in Fig. 1 using representative bulk measurements with known composition, including the final state of the samples once all ethanol is evaporated. The exact trajectory of the individual droplet compositions during evaporation is not known, and will vary with time throughout the suspension volume, but microscopic observations of the number of phases present at intermediate times are consistent with the bulk phase data in Fig. 1. The transformation time scale is broadly adjustable from minutes to hours by varying the ethanol removal rate, enabling *in situ* study.

Fig. 2a shows the change of a spherical droplet into a polyhedron over time, just as the droplet liquid phase has begun to form liquid crystalline facets. As ethanol diffuses out of the droplet and water diffuses in, surface facets stabilize and grow to form a symmetric, truncated octahedron. The liquid crystalline phase grows within the droplet,[46] increasing droplet elasticity and dominating the droplet's interfacial tension to preserve a non-spherical faceted shape. The last image in Fig. 2a indicates that the final particle size, yellow area, reflects the initial droplet size, red area. Only a small amount of shrinkage occurs as the liquid crystal particle forms, enabling control of particle size in, for example, a microfluidic process. The micrographs in Fig. 2a indicate the particles are three-dimensionally symmetric, as facets are visible on the far side of the transparent polyhedron. Formation in a low-viscosity continuous phase fluid with a yield stress, $\sigma_y \sim 0.5$ Pa,[52] immobilizes the particle, allowing three-dimensional growth, without altering its symmetry. The process is thus distinct from isotropic drop growth in a liquid crystalline phase[53,54] as well as crystal growth in solid-like gels.[55] Suspension in the dilute yield

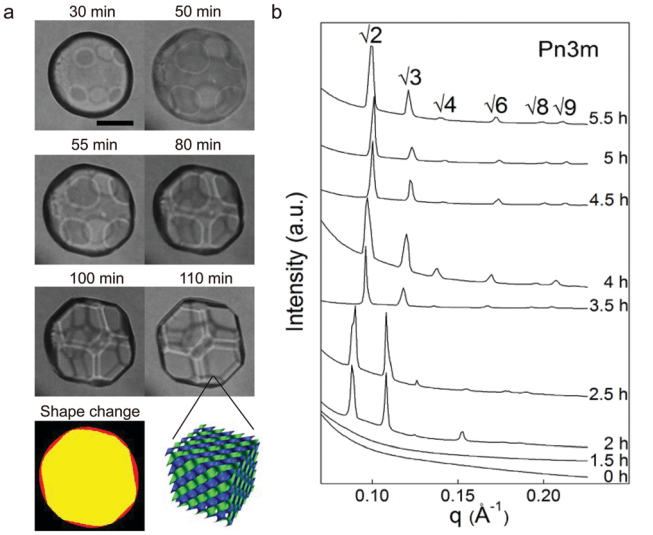

Fig. 2 (a) Evolution of a precursor droplet into a faceted polyhedral particle as ethanol is removed. A rendering of the bicontinuous phase structure is shown as inset to the last particle micrograph. The composition of the precursor solution is 55% w/w monoolein, 25% ethanol, and 20% water. (b) Evolution of the molecular structure of identical droplets measured by SAXS. The drops transform into bicontinuous cubic liquid crystalline structures on a time scale similar to the droplet in (a), though slower because of mass transport limitations. In each experiment, the aqueous MFC continuous phase contains 25% v/v ethanol. Scale bar is 50 μm.

stress fluid enables growth of faceted shapes without a need for a solid substrate[43,56] or close-packing of droplets.[22] Such a matrix is flexible enough to allow continuous production of droplets[48] while preserving the growing crystal symmetry. An additional benefit of the yield stress matrix is its immobilization of the droplet for further analytical interrogation with techniques such as SAXS.

Although we do not have a way of determining the composition of the individual droplets, we can document the rate at which mass is lost during the evaporation process. Such measurements establish the effect of the different evaporation driving forces used as well as allowing others to duplicate the process and tune the kinetics of the particle phase transition. We plot in Fig. 3 measurements of the mass loss as a function of time during static evaporation of ethanol from the suspensions. Three stages are observed: an initial linear stage, a transitional stage, and a final linear stage, identical to similar studies of solvent evaporation from a pre-hexagonal phase emulsion.[57] The initial linear part of the curve corresponds to the evaporation of both ethanol and water, and the slope decreases with time as the ethanol is depleted. The final stage is also linear with a smaller slope, as evaporation of ethanol has finished and only water evaporates at this stage. The intersection of the two linear regions provides an estimate of the characteristic time for completion of the particulate phase transition.[57] Three samples are plotted in Fig. 3 for different ethanol levels in the diluting fluid that alter the evaporation rate and allow tuning of the kinetics of the transition. In Fig. 3a, a diluting fluid with 33 wt% ethanol has the highest volatility

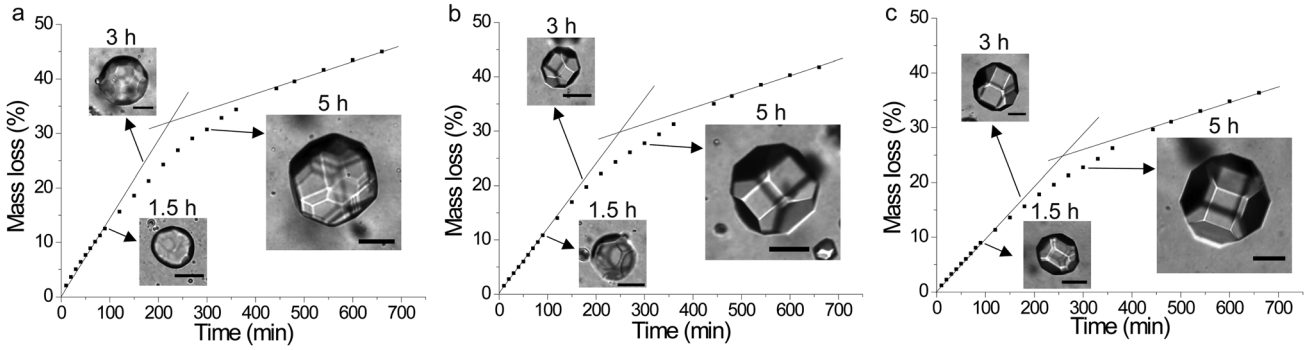

Fig. 3 Relative mass loss as a function of time during the transition process from droplets to particles for diluting solutions with ethanol content of (a) 33 wt%, (b) 25 wt% and (c) 20 wt%, corresponding to diluting solution compositions marked B, C, and D on Fig. 1. Best-fit lines are drawn for the initial and final linear regions. Inset microscopy images show particles at various stages of crystallization. Scale bar is 50 μm.

and the highest initial evaporation rate, obtained from a best-fit line to be 2.7 mg min^{-1}. The systems with lower ethanol levels have lower initial evaporation rates of 2.3 mg min^{-1} for a fluid containing 25 wt% ethanol, Fig. 3b, and 1.9 mg min^{-1} for a fluid with 20 wt% ethanol, Fig. 3c. Micrographs of representative particles are included as insets in Fig. 3 to emphasize the stage of formation of faceted structures as evaporation proceeds. The three systems form particles with essentially the same shape, a truncated octahedron, although diluting with a 33 wt% ethanol system causes a number of additional small facets to form because of the faster evaporation, and thus phase transition, rate. All other experiments used a diluting fluid containing 25 wt% ethanol and evaporation occurred at the same rate as the sample in Fig. 3b.

The reason for the formation of droplet facets in Fig. 2a is the underlying mesophase structure's cubic liquid crystalline symmetry. We verify structural contributions to particle shape using SAXS data for a precursor emulsion slowly evolving into faceted particles *via* evaporative ethanol removal from the sample cell. Fig. 2b shows the evolution of the dispersion's scattering peaks for the dispersion, indicating transformation into the highly ordered double-diamond bicontinuous cubic phase, V_2, *Pn3m*. Structural classification is made based on the six peaks at q ratios of $\sqrt{2}$, $\sqrt{3}$, $\sqrt{4}$, $\sqrt{6}$, $\sqrt{8}$, and $\sqrt{9}$. The lattice parameter, calculated according to the q values, decreases significantly from 10.0 nm at 2 h to 8.9 nm at 4.5 h. The smaller size of the unit cells indicates a more condensed structure and is a key indicator of the growth-by-redistribution process.[46] Analogous to solid structures, the soft polyhedra exhibit shapes consistent with their underlying self-assembly, specifically the symmetry onto which the formed bilayer intrinsically folds to form the bicontinuous inverse cubic phase. Here, solid-like rheology preserves the shape-structure relationship of traditional solid crystal formation in a more flexible, tunable liquid crystalline matrix. The rate of polyhedron formation is set by the rate of phase transformation and can be controlled by adjusting the rate of solvent removal.

Control of shape is central to the development of faceted particles for a specific application, or to create a particular structure *via* self-assembly. The single, underlying symmetry of the cubic liquid crystals studied here can produce a wide range of polyhedral particles depending on the relative growth rates of different facets. For convenience, we refer to specific crystal faces using the Miller index, (*hkl*), indicating three indices that are the inverse intercepts of a face's location with three-dimensional spatial axes.[58] Different facets have different associated energy states, partially dictating their stability and ease of formation. Fig. 4 shows the pathway to produce at least six distinct shapes, depending on the kinetics of individual face growth, as regulated by experimental conditions. Starting from a truncated octahedron, the most energetically stable form of an fcc liquid crystal,[19] growth of the (100) face moves the shape increasingly toward a true octahedron, Fig. 4 top path. The energy is the smallest for (111) facets and the largest for (110) facets in a cubic liquid crystal with *Pn3m* symmetry.[41] The highest energy facets tend to grow fastest in their perpendicular direction, often eliminating high-energy facets and maximizing surface area of low-energy facets, although liquid crystals can defy these expectations.[45,59] Similarly, growth of the (111) and then (110) faces moves the truncated octahedron through increasingly cubic shapes, to a cuboctahedron, a truncated cube, then a true cube, as we see in Fig. 4 bottom path. Synthesizing each of these shapes as soft particles is then a matter of determining the conditions that drive formation of the desired form.

In order to demonstrate the flexibility of this method for forming soft polyhedra, the following results demonstrate control of particle shape using several experimental variables: precursor droplet size, solubilized and adsorbed additives, and anisotropic composition and deformation.

3.1 Precursor droplet size

A number of polyhedra are shown in Fig. 5 that exhibit a distinct difference in shape, depending on precursor droplet size, in a single experiment. Octahedra form from precursor droplets smaller than 50 μm, as we see in Fig. 5a. Truncated octahedra, Fig. 5b, form from larger droplets in the size range 50–100 μm. Even larger droplets, >100 μm, produce truncated octahedra as well, Fig. 5c, but many more minor facets are visible. A similar stepped growth phenomenon at the surface of hemispherical droplets was reported by Pieranski and coworkers.[45,56]

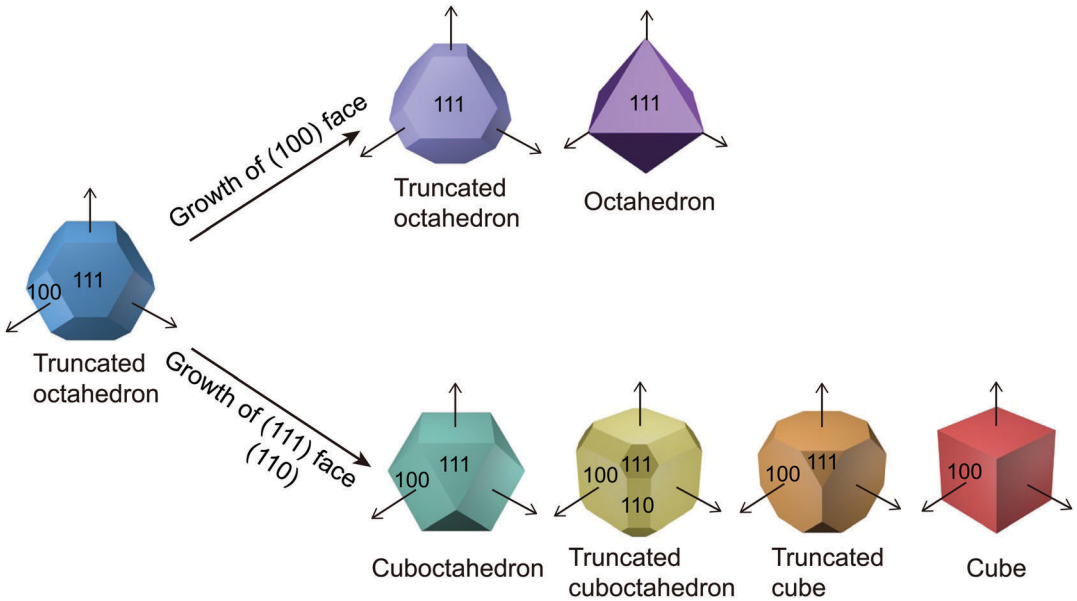

Fig. 4 Different polyhedra shapes can be produced by control of selective face growth from a single cubic liquid crystalline *Pn3m* symmetry.

The highly elastic cubic phase is uniquely able to stabilize many major and minor facets because its surface energy-to-elasticity ratio is about five times the phase's lattice spacing.[44] As a result, elastic energy is spent to gain surface energy and the minor facets are more stable than in harder crystal systems. Unlike conventional solution crystallization, that obtains monocrystals from the bulk solution, these particles draw on just their internal liquid volume to form a liquid crystalline polyhedron: growth-by-redistribution.[45,56] The starting volume will then limit the extent of face growth: smaller droplets with higher curvature will require a smaller amount of growth for the (100) face to disappear completely and produce an octahedron. We see octahedra forming below a size of 50 μm in Fig. 5a. The shape of the particles is thus linked to precursor droplet size as a result of face growth kinetics, meaning processes like microfluidics can control the size and shape produced. Nanoparticles will have the fastest transport rates of solvent into or out of the particle, allowing growth of (111) face to completely dominate. As a result, we would expect nanodroplets in this system to transform into octahedra but we have not studied this length scale in detail.

Increasing temperature at a fixed size produces an analogous result to varying droplet size. Most particles formed at 25 °C are truncated octahedra. At 35 °C, the particles more closely resemble octahedra, with larger (111) and smaller (100) faces,

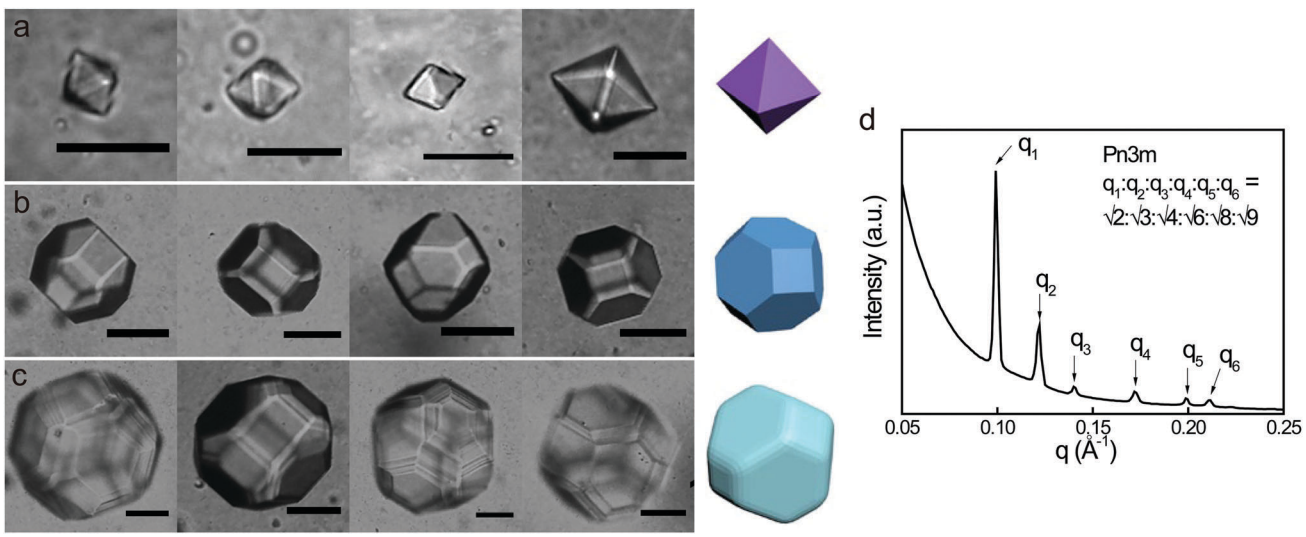

Fig. 5 Particles with different shapes based on the size of the precursor emulsion droplet. Each row shows four different examples of: (a) octahedra, smaller than 50 μm, scale bar is 50 μm; (b) truncated octahedra, smaller than 100 μm, scale bar is 50 μm; (c) truncated octahedra with visible minor facets, larger than 100 μm, scale bar is 30 μm. (d) SAXS results indicate that all the shapes have the same cubic liquid crystalline structure, *Pn3m* symmetry. The composition of precursor droplets and the ethanol content of the diluting solution match the conditions in Fig. 2.

while at 45 °C true octahedra form. Higher temperatures promote faster diffusion and increase face growth rates, more rapidly eliminating the high-energy (100) face.

Altering the ethanol concentration in the diluting solution, while keeping the precursor unchanged, also affects the final shape formed. For example, by increasing the level of ethanol, the shape of the resulting polyhedra is not changed significantly but the amount of small minor facets increases, reducing overall facet quality, as in Fig. 5c. Starting from a higher ethanol level in the phase diagram coincides with a change in the slope of the relevant phase coexistence line in the phase diagram,[46] allowing more face growth to occur as the ethanol is removed. A volume ratio of 20% v/v ethanol turns precursor droplets into sharply-faceted truncated octahedra, consistent with the effect of larger starting droplets seen in Fig. 5b. If the ethanol concentration in diluting liquid is too small, <17% v/v, the system moves immediately from the emulsion region of Fig. 1 to the cubosome region, producing only irregular chunks of cubic phase without shape control. Particles with polyhedral shapes form best when the diluting solution has an ethanol content >17% v/v and <33% v/v. Additional shapes can be produced using other methods to control the face growth dynamics.

3.2 Additive effects on surface and molecular packing

Cubic liquid crystalline molecular structure is altered[60] by added solutes,[61,62] salts,[63] changes in pH in the presence of ionizable additives[64] and temperature.[65,66] Molecules solubilized into the liquid crystal can impact the molecular packing of the phase, producing relatively minor changes in lattice spacing or more major phase transitions. Additives are often used, for example, to effect changes in solute release rates,[67] or to make very viscous phases easier to process.[40] We apply this concept here to broaden the range of polyhedral shapes of cubic liquid crystalline microparticles by changing the dominant faces in the underlying cubic symmetry. Pluronic F127 is an amphiphilic triblock co-polymer, PEO_{99}–PPO_{67}–PEO_{99}, that is known to insert into the monoolein bilayer and cause a molecular structural transition from *Pn3m* to *Im3m* symmetry in bulk cubic phases.[41,61,68]

We see such a transition here for our dispersed microparticles formed from precursor solution with small amounts of F127 added. The diluting solution in all cases contained water with 25% v/v ethanol and 0.1% w/w MFC. Fig. 6a and c show polyhedra formed at 1% and 2% w/w F127 of the precursor solution while Fig. 6b and d show the SAXS data for the corresponding dispersions. At 1% w/w F127, cuboctahedra form in contrast to the regular and truncated octahedral shapes in Fig. 5 without added F127. The molecular structure reflects two-phase coexistence between *Pn3m* and *Im3m* cubic phases based on the indexed scattering visible for each phase, with the reflections attributable to the *Im3m* structure dominating those of the *Pn3m* phase in Fig. 6b. When F127 was increased to 2% w/w in the precursor solution, the SAXS profile showed three peaks indicating *Im3m* symmetry, demonstrating that the self-assembled structure had fully formed a single cubic phase at these F127 levels. When the *Im3m* phase dominates, the

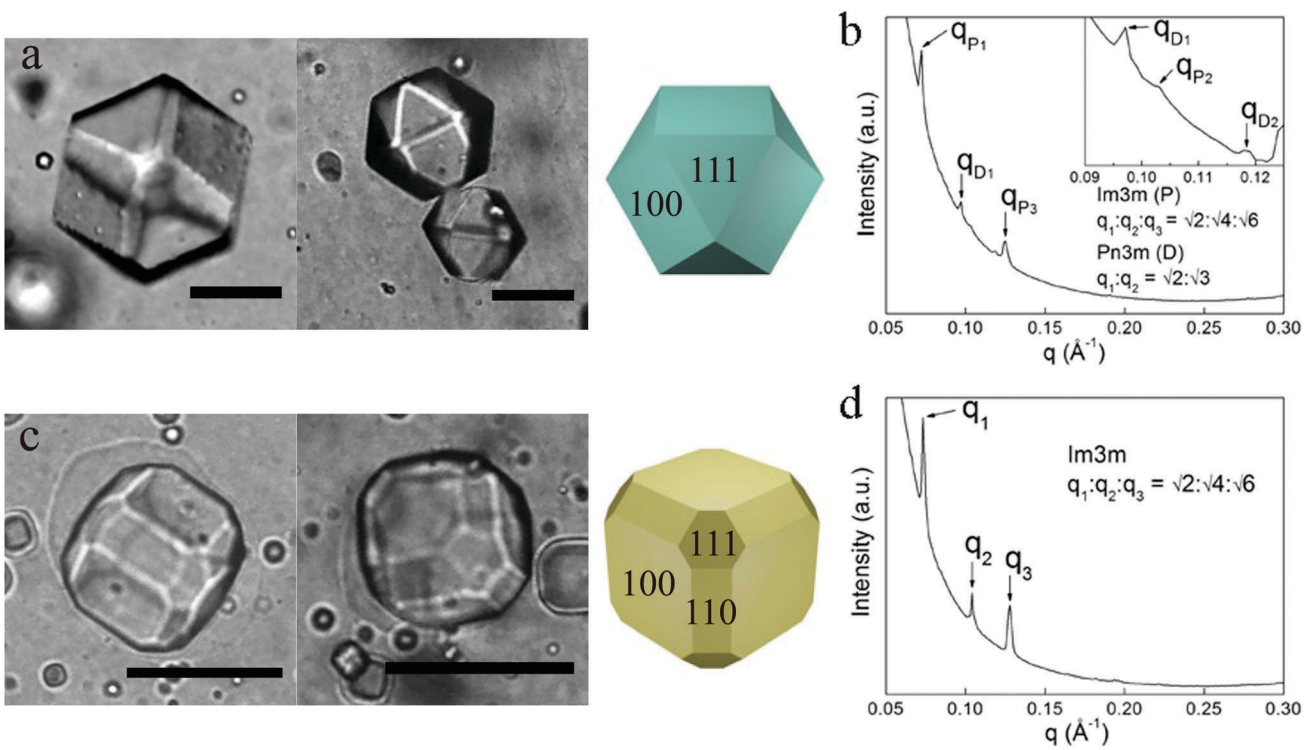

Fig. 6 Microscope images, 3D model, and SAXS peaks for particles with added Pluronic F127 polymer. The F127 is present at 1% w/w in (a) and (b) and at 2% w/w in (c) and (d), while all other precursor ingredients are in the same proportions as before. Scale bar is 50 μm. The diluting solution contains 0.1% w/w MFC.

particles are truncated cuboctahedra with added (110) faces besides the (100) and (111) faces formed in other shapes. Droplets on a substrate form an additional (211) face[46] but we did not observe such structures here. Interestingly, F127 is known to form and stabilize lamellar phase vesicles in similar systems[40] and the particles in Fig. 6c show apparent vesicular membrane "halos" surrounding the largest particles. Vesicles are not seen in other samples, and do not seem to detract from the ability to form polyhedral shapes here. Solubilization of F127 into the liquid crystal clearly provides additional control over dominant face growth and final polyhedral shape by transformation of the cubic phase space group. This may be why cubes are mostly observed when nanoparticle cubosomes, ~50–200 nm, are formed by fragmentation of bulk cubic phase in the presence of F127.[40,69] Given the surface nature of the initial facet formation, we might also expect effects by adsorbed additives.

Crosslinked polyacrylic acid particles are known to swell in water, when neutralized, to form microgels varying in size from 800–1200 nm. The microgels can interact with nonionic surfactants *via* adsorption or partitioning of some surfactants into the microgels.[70] Here we exploit this property by growing polyhedral particles in aqueous polyacrylate microgels, with or without MFC, in order to understand the effects on particle shape. Fig. 7a shows particles grown in 0.08% w/w microgels while Fig. 7b shows particles formed in 0.03% w/w microgels mixed with 0.05% w/w MFC. The particles formed cuboctahedra, truncated cubes, and cubes, distinct from the octahedra and truncated octahedra formed in MFC, Fig. 5. Microgels likely adsorb at (100) faces, slowing their growth and causing (111) faces to disappear. In Fig. 7c, the SAXS data for the particles in Fig. 7a indicate that the phase of the liquid crystal is not changed. Appreciable solubilization of the polymer is therefore unlikely and the effects on polyhedron shape are more likely due to adsorption effects. Adding precursor solution to a mixture of microgels and MFC containing 25% v/v ethanol forms particles, Fig. 7b, with a mixture of shapes like those in Fig. 5 and 7a, indicating smaller effects of adsorption at lower microgel concentrations. Movie S1 (ESI†) shows two cubes that have formed from droplets and are rotating due to local interfacial tension gradients, highlighting the transparency and symmetry of the shapes.

We see in Fig. 5–7 that polyhedral shapes can be distinctly altered as they grow from spherical precursor droplets by favoring growth or disappearance of certain crystal faces. Such behavior is in good agreement with the overall pathways in Fig. 4. The range of shapes produced from a simple system using common techniques like size control, and small amounts of additives, is surprisingly broad. If the remarkable isotropic symmetry of the shapes in Fig. 5–7 results from isotropic precursor shapes and environmental compositions, we hypothesize that more anisotropic initial conditions may provide additional degrees of shape control as the crystals grow. Polyhedral particles with broken symmetry could enable validation of theoretical structures predicted to form from Voronoi particles,[15] and provide more diverse building blocks of larger hierarchical structures.

3.3 Anisotropy in composition and deformation

A simple means of varying the growth of crystals in precursor emulsion droplets is to arrange a gradient in driving force across the droplets. An example is at the air–liquid interface of an emulsion where removal rates are faster from the top than the bottom. Fig. 8 shows several examples of anisotropic polyhedra formed with a shape that varies from one side to the other, in some cases octahedra morphing into what more resembles a truncated octahedron. Such shapes are not controlled or reproducible to any degree at this stage, but indicate the continuity of shape possible in this system even with non-uniform driving forces. An analogous effect was demonstrated for cubic liquid crystals in another lyotropic system using a temperature gradient.[71]

A second anisotropic constraint on final polyhedral shape is the starting shape of the precursor droplet. Precursor droplets can be deformed into ellipsoids by extensional deformation of the surrounding fluid if the continuous phase fluid has a yield stress on the order of $\sigma_y \sim$ 10–50 Pa and can offset interfacial forces[72] trying to return the droplets to a spherical shape.

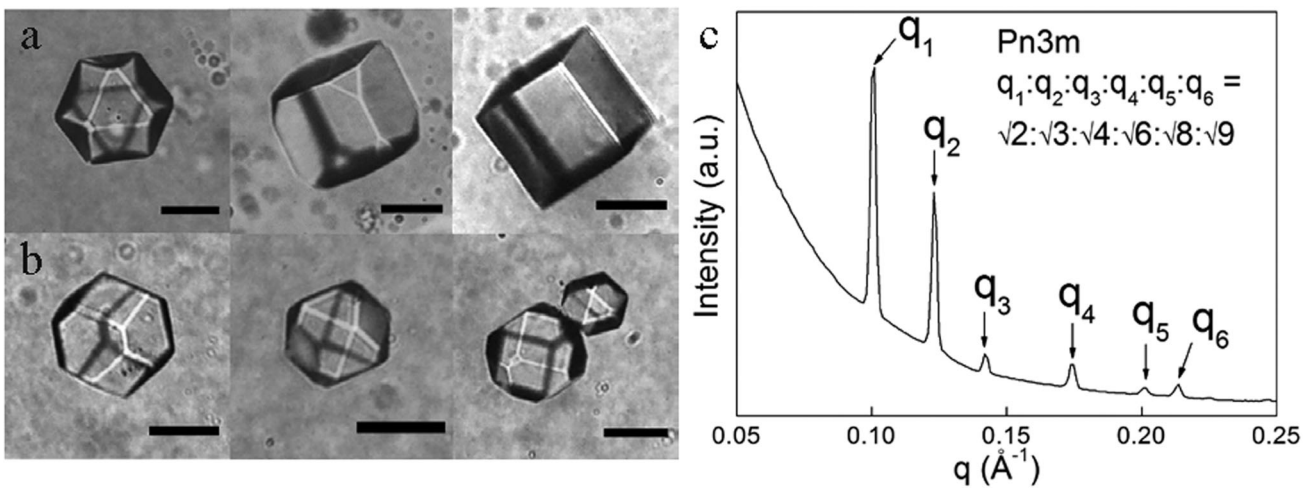

Fig. 7 (a) Different shapes formed in aqueous 0.08% polyacrylate microgel suspensions and (b) 0.03% w/w aqueous microgels mixed with 0.05% MFC in the diluting solution. (c) SAXS result of particles formed in (a). Each row shows multiple examples. Scale bar is 50 μm.

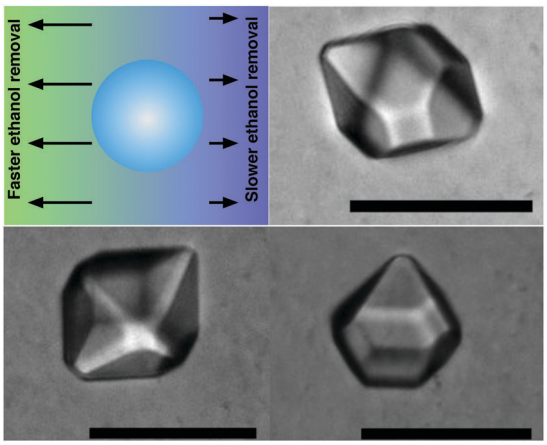

Fig. 8 Polyhedral particles with shapes intermediate between more regular forms, formed using controlled, but anisotropic, growth rates. Scale bar is 50 μm.

Such effects have been used to mold nematic droplets[26] and to arrest the relaxation of Pickering emulsion droplets.[25] When the ethanol is removed from the deformed droplets, we see growth of polyhedral shapes as in the spherical case, Fig. 2, but now the symmetry of the facets is superimposed on the ellipsoidal form, Fig. 9. Several modes of shape adaptation are seen for the polyhedra grown on ellipsoids. Facets are sometimes stretched along the ellipsoid long axis. Additional small minor facets are also common, as well as some blending of different shapes like the particles in Fig. 8. It is fascinating to see the increased aspect ratios of the normally isotropic polyhedra in Fig. 9. Initial deformation of the precursor droplet offers another way to tailor the dimension and relative orientation of facets while retaining their apparent surface uniformity.

It is worth emphasizing that, though appearing quite solid in their faceted, polyhedral form, these particles are still liquid crystals with a moderate deformability. Fig. 10 demonstrates this *via* a sequence of microscopy images showing a polyhedral particle, Fig. 10a, being aspirated by a microcapillary. The particle deforms to the dimensions of the capillary, Fig. 10b, but can be seen to retain some of the faceting that had already formed.

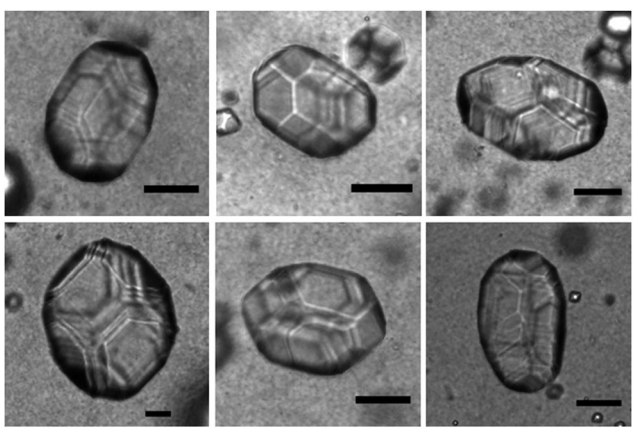

Fig. 9 Particles grown from droplets elongated into ellipsoids by deformation of the diluting solution yield stress fluid. Scale bar is 50 μm.

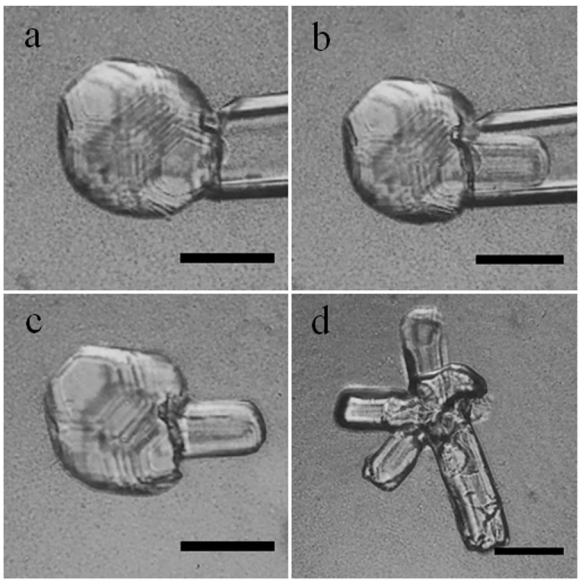

Fig. 10 Polyhedral particle aspirated by a microcapillary to demonstrate the permanent deformation that occurs as a result of flow of the cubic phase at high stresses. Movie S2 (ESI†) shows the process. Scale bar is 50 μm.

Once released from the capillary, Fig. 10c, the particle's significant yield stress ensures that it retains all of its original shape except where it was aspirated and molded into a cylindrical appendage. Further deformation can then be carried out as well, vastly reshaping and destroying the original symmetry of the polyhedron, Fig. 10d. Although a crude example, Fig. 10 demonstrates the potential for another type of shape constraint on the underlying molecular structure providing polyhedral symmetry and faceting. The enhanced flexibility of forming faceted particles *via* liquid crystalline growth adds new possibilities

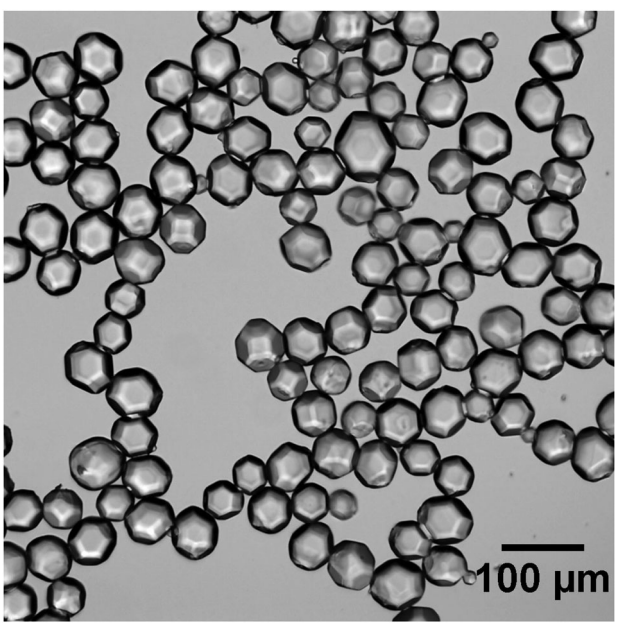

Fig. 11 Micrograph of multiple soft truncated octahedral particles formed using this process.

to the shapes normally achieved by solid crystal growth processes *via* an emulsion precursor.

Because the particles are easily produced from a readily prepared emulsion by simple evaporation, numerous polyhedra can be formed at once. Fig. 11 shows an image of about 125 truncated octahedra whose size variability reflects that of their precursor emulsion. Preliminary production of such particles using millifluidic flow yields a size distribution with some variability as a result of the low interfacial tension between the two equilibrating liquid phases. Image analysis of the particles in Fig. 11 gives a mean size of 52.2 μm with a standard deviation of 9.6 μm. We are still studying ways to produce truly monodisperse suspensions using this process.

4 Conclusions

We have demonstrated the flexible creation of soft polyhedral particles with a range of shapes based on variations of the cubic symmetry group and different modes of face growth within the groups. Precursor emulsion droplets of lipid and solvent are the basis for growth, *via* solvent removal, into faceted, highly elastic, soft three-dimensional shapes in a yield stress fluid. The rate of face growth can be varied using straightforward variables like droplet size, temperature, and solubilized and adsorbed additives, to control shape. Time scales of particle growth vary from minutes to hours depending on the driving force for mass transport. Arrest of the system in a desired shape is possible by halting solvent removal, and we are pursuing the templating and polymerization of these shapes to produce solid particles.

The polyhedra created here are unique in that they possess solid-like faceting and shape but also have a biologically-compatible liquid bicontinuous nanostructure that can encapsulate a wide range of solutes for delivery, reaction, and uptake functions. As a result, the particles can apply shape and structural properties over length scales from the molecular to the millimetric in one particle. The technique of soft polyhedra production has potential for new application areas like additive manufacturing and the creation of metamaterials, especially given the unique acoustic properties of the cubic phases.[32] The method may also provide a way to study other links between internal, molecular-scale structure and packing and the overall microscopic shape of particles. Far more complex faceting patterns could likely be produced on these particles by applying the insights of past single crystal phase mapping work,[46] as well as the anisotropic methods explored here. Microfluidic processes are currently being developed to produce these particles in a more continuous fashion so that their self-assembly behavior can be explored. We also plan to investigate the shape-changing abilities of these particles, given their elasticity and responsiveness, as this is another promising approach to complex self-assembly.[73]

Conflicts of interest

There are no conflicts of interest to declare.

Acknowledgements

Brad Forrest (DuPont/Danisco) is thanked for donating the glycerol monoolein. Financial support for HW's PhD from the UNSW School of Chemical Engineering is gratefully acknowledged. SAXS data were obtained on the SAXS/WAXS beamline at the Australian Synchrotron. Dr Matthew Lynch (Procter & Gamble Company), Ms Mina Adeline Benzie, and Associate Professor Anne Prescott (University of Technology Sydney) shaped our early understanding of polyhedra.

References

1 S. A. Cummer, J. Christensen and A. Alù, *Nat. Rev. Mater.*, 2016, **1**, 16001.
2 J. R. Royer, G. L. Burton, D. L. Blair and S. D. Hudson, *Soft Matter*, 2015, **11**, 5656–5665.
3 J. Champion and S. Mitragotri, *Proc. Natl. Acad. Sci. U. S. A.*, 2006, **103**, 4930.
4 P. Decuzzi, R. Pasqualini, W. Arap and M. Ferrari, *Pharm. Res.*, 2009, **26**, 235–243.
5 E. Gavze and M. Shapiro, *Int. J. Multiphase Flow*, 1997, **23**, 155–182.
6 J. Park and J. E. Butler, *Macromolecules*, 2010, **43**, 2535–2543.
7 B. R. Smith, P. Kempen, D. Bouley, A. Xu, Z. Liu, N. Melosh, H. Dai, R. Sinclair and S. S. Gambhir, *Nano Lett.*, 2012, **12**, 3369–3377.
8 R. Toy, P. M. Peiris, K. B. Ghaghada and E. Karathanasis, *Nanomedicine*, 2014, **9**, 121–134.
9 S. Glotzer and M. J. Solomon, *Nat. Mater.*, 2007, **6**, 557–562.
10 P. F. Damasceno, M. Engel and S. C. Glotzer, *Science*, 2012, **337**, 453–457.
11 J. A. Millan, D. Ortiz and S. C. Glotzer, *Soft Matter*, 2015, **1**, 1386–1396.
12 G. van Anders, N. K. Ahmed, R. Smith, M. Engel and S. C. Glotzer, *ACS Nano*, 2013, **8**, 931–940.
13 K. L. Young, M. L. Personick, M. Engel, P. F. Damasceno, S. N. Barnaby, R. Bleher, T. Li, S. C. Glotzer, B. Lee and C. A. Mirkin, *Angew. Chem., Int. Ed.*, 2013, **52**, 13980–13984.
14 J. A. Millan, D. Ortiz, G. van Anders and S. C. Glotzer, *ACS Nano*, 2014, **8**, 2918–2928.
15 B. A. Schultz, P. F. Damasceno, M. Engel and S. C. Glotzer, *ACS Nano*, 2015, **9**, 2336–2344.
16 D. Dendukuri, S. Gu, D. Pregibon, T. Hatton and P. Doyle, *Lab Chip*, 2007, **7**, 818–828.
17 T. Merkel, K. Herlihy, J. Nunes, R. Orgel, J. Rolland and J. DeSimone, *Langmuir*, 2009, 557.
18 G. Vernizzi and M. O. de la Cruz, *Proc. Natl. Acad. Sci. U. S. A.*, 2007, **104**, 18382–18386.
19 Y. Xia, Y. Xiong, B. Lim and S. E. Skrabalak, *Angew. Chem., Int. Ed.*, 2009, **48**, 60–103.
20 M. L. Personick and C. A. Mirkin, *J. Am. Chem. Soc.*, 2013, **135**, 18238–18247.
21 R. A. Brady, N. J. Brooks, P. Cicuta and L. Di Michele, *Nano Lett.*, 2017, **17**, 3276–3281.

22 J. Fan, S.-H. Kim, Z. Chen, S. Zhou, E. Amstad, T. Lin and D. A. Weitz, *Small*, 2017, 1701256.
23 J. J. Crassous, A. M. Mihut, L. K. Månsson and P. Schurtenberger, *Nanoscale*, 2015, **7**, 15971–15982.
24 A. Pawar, M. Caggioni, R. Ergun, R. Hartel and P. Spicer, *Soft Matter*, 2011, **7**, 7710.
25 C. J. Burke, B. L. Mbanga, Z. Wei, P. T. Spicer and T. J. Atherton, *Soft Matter*, 2015, **11**, 5872–5882.
26 E. Pairam and A. Fernandez-Nieves, *Phys. Rev. Lett.*, 2009, **102**, 234501.
27 A. Pawar, M. Caggioni, R. Hartel and P. Spicer, *Faraday Discuss.*, 2012, **158**, 341–350.
28 E. Pairam, J. Vallamkondu, V. Koning, B. C. van Zuiden, P. W. Ellis, M. A. Bates, V. Vitelli and A. Fernandez-Nieves, *Proc. Natl. Acad. Sci. U. S. A.*, 2013, **110**, 9295–9300.
29 D. Lootens, C. Vautrin, H. Van Damme and T. Zemb, *J. Mater. Chem.*, 2003, **13**, 2072–2074.
30 N. Denkov, S. Tcholakova, I. Lesov and D. Cholakova, *Nature*, 2015, **528**, 392–396.
31 S. Guttman, Z. Sapir, M. Schultz, A. V. Butenko, B. M. Ocko, M. Deutsch and E. Sloutskin, *Proc. Natl. Acad. Sci. U. S. A.*, 2016, **113**, 493–496.
32 J. L. Jones and T. C. B. McLeish, *Langmuir*, 1995, **11**, 785–792.
33 S. Radiman, C. Toprakcioglu and T. McLeish, *Langmuir*, 1994, **10**, 61–67.
34 C. Drummond, *Curr. Opin. Colloid Interface Sci.*, 2000, **4**, 449–456.
35 B. J. Boyd, D. V. Whittaker, S.-M. Khoo and G. Davey, *Int. J. Pharm.*, 2006, **309**, 218–226.
36 B. Boyd, S.-M. Khoo, D. V. Whittaker, G. Davey and C. J. H. Porter, *Int. J. Pharm.*, 2007, **340**, 52–60.
37 C. Fong, T. Le and C. J. Drummond, *Chem. Soc. Rev.*, 2012, **41**, 1297–1322.
38 X. Mulet, B. J. Boyd and C. J. Drummond, *J. Colloid Interface Sci.*, 2013, **393**, 1–20.
39 J. Gustafsson, H. Ljusberg-Wahren, M. Almgren and K. Larsson, *Langmuir*, 1996, **12**, 4611–4613.
40 P. Spicer, K. Hayden, M. Lynch, A. Ofori-Boateng and J. Burns, *Langmuir*, 2001, **17**, 5748–5756.
41 M. Nakano, T. Teshigawara, A. Sugita, W. Leesajakul, A. Taniguchi, T. Kamo, H. Matsuoka and T. Handa, *Langmuir*, 2002, **18**, 9283–9288.
42 W. K. Fong, S. Salentinig, C. A. Prestidge, R. Mezzenga, A. Hawley and B. J. Boyd, *Langmuir*, 2014, **30**, 5373–5377.
43 J. Bechhoefer, L. Lejcek and P. Oswald, *J. Phys. II*, 1992, **2**, 27–44.
44 P. Nozieres, F. Pistolesi and S. Balibar, *Eur. Phys. J. B*, 2001, **24**, 387–394.
45 P. Pieranski, P. Sotta, D. Rohe and M. Imperor-Clerc, *Phys. Rev. Lett.*, 2000, **84**, 2409–2412.
46 L. Latypova, W. Góźdź and P. Pieranski, *Eur. Phys. J. E: Soft Matter Biol. Phys.*, 2013, **36**, 88–111.
47 Y. D. Dong, A. J. Tilley, I. Larson, M. J. Lawrence, H. Amenitsch, M. Rappolt, T. Hanley and B. J. Boyd, *Langmuir*, 2010, **26**, 9000–9010.
48 R. Shah, H. Shum, A. Rowat, D. Lee, J. Agresti, A. Utada, L. Chu, J. Kim, A. Fernandez-Nieves, C. Martinez and D. Weitz, *Mater. Today*, 2008, **11**, 18–27.
49 C. Ohm, C. Serra and R. Zentel, *Adv. Mater.*, 2009, **21**, 4859–4862.
50 N. M. Kirby, S. T. Mudie, A. M. Hawley, D. J. Cookson, H. D. Mertens, N. Cowieson and V. Samardzic-Boban, *J. Appl. Crystallogr.*, 2013, **46**, 1670–1680.
51 S. Mudie, *Scatterbrain software*, 2017, www. synchrotron.org.au.
52 H. Emady, M. Caggioni and P. Spicer, *J. Rheol.*, 2013, **57**, 1761.
53 P. Sotta, *J. Phys. II*, 1991, **1**, 763–772.
54 M. Lynch, K. Kochvar, J. Burns and R. Laughlin, *Langmuir*, 2000, **16**, 3537–3542.
55 M. Robert and F. Lefaucheux, *J. Cryst. Growth*, 1988, **90**, 358–367.
56 P. Pieranski, L. Sittler, P. Sotta and M. Imperor-Clerc, *Eur. Phys. J. E: Soft Matter Biol. Phys.*, 2001, **5**, 317–328.
57 I. Martiel, L. Sagalowicz, S. Handschin and R. Mezzenga, *Langmuir*, 2014, **30**, 14452–14459.
58 N. H. Hartshorne and A. Stuart, *Practical optical crystallography*, Elsevier, 1969.
59 P. Pieranski, M. Bouchih, N. Ginestet and S. Popa-Nita, *Eur. Phys. J. E: Soft Matter Biol. Phys.*, 2003, **12**, 239–254.
60 A. Yaghmur and O. Glatter, *Adv. Colloid Interface Sci.*, 2009, **147-148**, 333–342.
61 Y.-D. Dong, I. Larson, T. Hanley and B. J. Boyd, *Langmuir*, 2006, **22**, 9512–9518.
62 J. Zhai, L. Waddington, T. J. Wooster, M.-I. Aguilar and B. J. Boyd, *Langmuir*, 2011, **27**, 14757–14766.
63 Q. Liu, Y.-D. Dong, T. L. Hanley and B. J. Boyd, *Langmuir*, 2013, **29**, 14265–14273.
64 R. Negrini and R. Mezzenga, *Langmuir*, 2011, **27**, 5296–5303.
65 W.-K. Fong, T. Hanley and B. J. Boyd, *J. Controlled Release*, 2009, **135**, 218–226.
66 X. Mulet, X. Gong, L. J. Waddington and C. J. Drummond, *ACS Nano*, 2009, **3**, 2789–2797.
67 S. Phan, W.-K. Fong, N. Kirby, T. Hanley and B. J. Boyd, *Int. J. Pharm.*, 2011, **421**, 176–182.
68 T. Landh, *J. Phys. Chem.*, 1994, **98**, 8453–8467.
69 S. B. Rizwan, Y.-D. Dong, B. J. Boyd, T. Rades and S. Hook, *Micron*, 2007, **38**, 478–485.
70 R. Barreiro-Iglesias, C. Alvarez-Lorenzo and A. Concheiro, *J. Controlled Release*, 2001, **77**, 59–75.
71 P. Pieranski, *Liq. Cryst.*, 2009, **36**, 1049–1069.
72 M. Caggioni, A. V. Bayles, J. Lenis, E. M. Furst and P. T. Spicer, *Soft Matter*, 2014, **10**, 7647–7652.
73 T. Nguyen, E. Jankowski and S. Glotzer, *ACS Nano*, 2011, **5**, 8892–8903.